Paper **CFDSC2013-188**,
21st Annual Conference of the CFD Society of Canada,
Sherbrooke, Canada, May 6-9, 2013.

Spectral Simulations of the Partial Reconnection Phenomena of Aircraft Wake Vortices

Guillaume Beardsell[1], Louis Dufresne[2], and Guy Dumas[1]

[1] *Laboratoire de Mécanique des Fluides Numérique, Département de Génie Mécanique Université Laval, Québec, QC, G1V 2V3, Canada*

[2] *Laboratoire de Thermofluide pour le Transport École de Technologie Supérieure, Montréal, QC, H3C 1K3, Canada*

Email: *Guillaume.Beardsell.1@ulaval.ca*

Abstract

Aircraft wake vortices represent a possible hazard for other aircrafts flying nearby, in particular on the outskirts of airstrips. In this work, partial reconnection of a simplified system of two unequal-strength vortices is studied in order to assess its impact on the longevity of the wake vortex system. A spectral method is used to carry out DNS (Direct Numerical Simulation) in order to study the reconnection of two orthogonal vortices for Reynolds number $(\Gamma/\nu) = 10^4$ following the approach of Boratav et al. [2]. Hyperviscous LES (Large Eddy Simulation) simulations are also executed to study partial reconnection for Reynolds numbers varying from 10^4 to 10^6. The internal structure of the main vortex is examined with a particular attention to the propagating vorticity perturbations. These structures are found to be very similar to what has been previously observed in the evolution of four-vortex systems [6]. Beyond the mechanisms of partial reconnection and its structures, methodological aspects with regards to the dimensions of the periodic domain and the use of hyperviscosity are discussed.

1 Introduction

In order to take off and fly, an airplane must generate a force equal to its weight. It is known that when a wing generates lift, it also generates a pair of counter-rotating vortices. These little "tornados" can be very powerful and their intensity is proportional to the weight of the aircraft [12], representing a potential hazard for other aircrafts flying nearby. These vortices are the cause of the delays between two takeoffs / landings in congested airports. The waiting time required between each aircraft is related to the intensity and persistence of these vortices. Dissipation of these structures depends heavily on hydrodynamic instabilities which are the source of fine turbulence in such flow. On their part, instabilities and the wake vortex dynamics depend very much on the internal structure of the vortices, the atmospheric turbulence and eventually the ground effects.

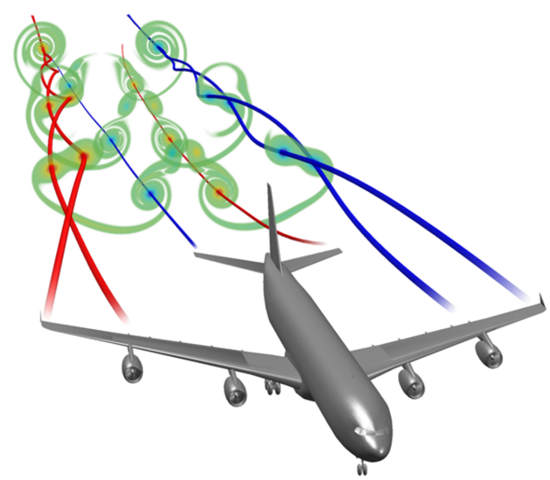

Figure 1: *Schematics of the four-vortex system created by an airplane when the tailplane generates downforce.*

Thorough understanding of these dynamics is very important to improve flight safety and to reduce airport congestion [3, 8, 11]. Partial reconnection occurs when a pair of counter-rotating vortices of varying intensity meet. This happens for example when the tailplane generates downforce at takeoff / landing. In addition to the wingtip vortices, the tailplane generates a second pair of weaker vortices. This creates a four-vortex system, as seen on Figure 1. Previous experiments have shown that the decay of similar vortex configurations is dominated by the medium wavelength instability, which deforms the weaker vortices into the so-called Omega loops, as seen on Figure 2 [10]. Also, it should be noted from Figure 2 that before the partial reconnection occurs, the secondary vortex is locally almost orthogonal to the main vortex. Recent studies [6] suggest that partial reconnection generates a large spectrum of small-scale turbulent structures that should sig-

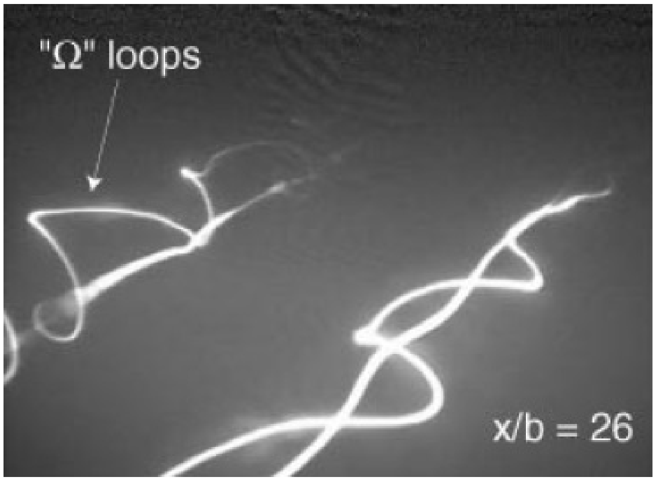

Figure 2: *Four-vortex system created by a triangular-flapped wing. Taken from "Experimental study of the instability of unequal strength counter-rotating vortex pairs" [10].*

nificantly increase the dissipation rate of the wake vortices. In this work, partial reconnection of a simplified system of two orthogonal, unequal-strength vortices is studied.

2 METHODOLOGY

In this work, a standard Fourier-Galerkin projection in the three Cartesian directions [4] is used to solve the conservative formulation of the incompressible Navier-Stokes equations in which a hyperviscous term has been added

$$\frac{\partial \mathbf{u}}{\partial t} + \nabla \cdot (\mathbf{u}\mathbf{u}) = -\nabla P + \nu \nabla \cdot \nabla \mathbf{u} - \nu_{hv} \nabla^{16} \mathbf{u}, \tag{1}$$

where $P = p/\rho$ is the reduced pressure. The incompressibility constraint

$$\nabla \cdot \mathbf{u} = 0 \tag{2}$$

is exactly satisfied by a reprojection of the velocity field onto a divergence free space. The Fourier expansion for velocity has the form

$$\mathbf{u}(\mathbf{x},t) = \sum_{\mathbf{k}} \hat{\mathbf{u}}(\mathbf{k},t) e^{i\mathbf{k}\cdot\mathbf{x}}, \tag{3}$$

where the wavenumber and position vectors are

$$\mathbf{k} = \{ k_x, k_y, k_z \} \qquad \mathbf{x} = \{ x, y, z \}$$

$$k_q = m_q \frac{2\pi}{L_q} \qquad -\frac{N_q}{2} + 1 \leq m_q \leq \frac{N_q}{2} \tag{4}$$

with q being an index standing for x, y or z, and L_q the size of the periodic domain in the q direction.

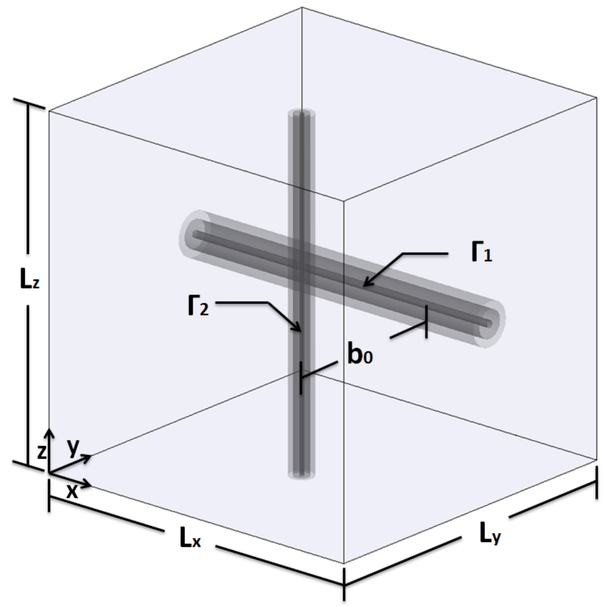

Figure 3: *Initial configuration for the two orthogonal, unequal-strength vortices. The figure shows vorticity isosurfaces* $\omega^* = [0.25, 0.5, 0.75]$.

A phase-shift procedure is implemented for dealiasing purposes and time integration is achieved using an explicit 3rd order Runge-Kutta scheme. Hyperviscosity (ν_{hv}) is introduced in order to stabilize the flow evolution at high Reynolds numbers and will be discussed later.

Dissipation rate per unit mass is computed as

$$\varepsilon = \frac{1}{V} \nu \int_{\mathbf{V}} \nabla \mathbf{u} \cdot \nabla \mathbf{u} \, dV + \frac{1}{V} \nu_{hv} \int_{\mathbf{V}} \nabla^8 \mathbf{u} \cdot \nabla^8 \mathbf{u} \, dV. \tag{5}$$

The initial radial vorticity distribution of each vortex is generated with a high-order formulation of the form

$$\omega(r) = \Gamma \frac{2\beta^4 R^4}{\pi (r^2 + \beta^2 R^2)^3} \tag{6}$$

where $\beta = 0.7788$, and in which Γ is the total circulation and R is the size of the vortex. Validation of the present spectral code with the results of Boratav et al. [2] has previously been presented in [5].

In this study, all quantities are normalized using the scales given by the inner-spacing b_0 and the main vortex circulation Γ_1 (see Figure 3). The radius of both vortices and the circulation of the secondary vortex are defined independently. The relation

$$\frac{\Gamma_2}{\Gamma_1} = \frac{R_2^2}{R_1^2} \tag{7}$$

is however enforced in order to ensure similar vorticity magnitude for both vortices. In this paper, all simulations are conducted with $\Gamma_2/\Gamma_1 = 0.3$ and $R_1/b_0 = 1$. Hence, $R_2/b_0 = \sqrt{0.3}$. Reference velocity and time are given by $V_{ref} = \Gamma_1/b_0$ and $t_{ref} = {b_0}^2/\Gamma_1$ respectively. Reynolds number is $Re = \Gamma_1/\nu$, where ν is the kinematic viscosity of the fluid. Throughout the text, non-dimensional time is given by $t^* = t/t_{ref}$.

As seen on Figure 3, the periodic box is characterized by its spatial dimensions (L_x, L_y, L_z). For a given box size, the number of collocation points in each direction (N_x, N_y, N_z) determines the resolution of the box. For all simulations, we have chosen

$$\frac{L_x}{N_x} = \frac{L_y}{N_y} = \frac{L_z}{N_z} \tag{8}$$

in order to avoid artificial anisotropic behaviour of the flow at the small scales. All present simulations are performed with cubic boxes, hence $L = L_x = L_y = L_z$ and $N = N_x = N_y = N_z$.

3 PARTIAL RECONNECTION PROCESS

Initially, unequal strength vortices are placed orthogonally in the periodic box, as seen in Figure 3. This configuration not being an equilibrium solution, no initial perturbation is needed to begin the partial reconnection process. The first instants of the phenomenon are characterised by the secondary vortex wrapping itself around the larger one, as seen on Figure 5a. While the secondary vortex is highly deformed, the main vortex remains almost intact in comparison. When the secondary vortex approaches the main vortex sufficiently, partial reconnection occurs, as seen on Figure 5b. This creates a circulation deficit on the main vortex and two circulation "steps" that move away from each other and eventually collide with their periodic images. Reconnection is characterized by the formation of small bridges (or fingers) of vorticity, as previously observed in other numerical simulations of vortex reconnection [2, 6].

This process leaves the main vortex weakened and disorganized, as seen on Figure 5c. When the traveling structures meet their periodic images, it causes an additional burst of small structures, as seen on Figure 5d. However, the focus of this paper is set on the partial reconnection itself; therefore any interaction with the neighbours is not desirable at this point. These interactions do exist in nature [10] and they appear to contribute significantly to the energy decay of the four-vortex system. They are thus certainly of interest for future work. From Figure 4 and Figure 5, one can see that the partial reconnection phenomenon produces a lot of small structures. This leads to increased dissipation, as seen on Figure 6, which compares the partial reconnection process to the normal viscous dissipation of the same vortices placed far away from each other.

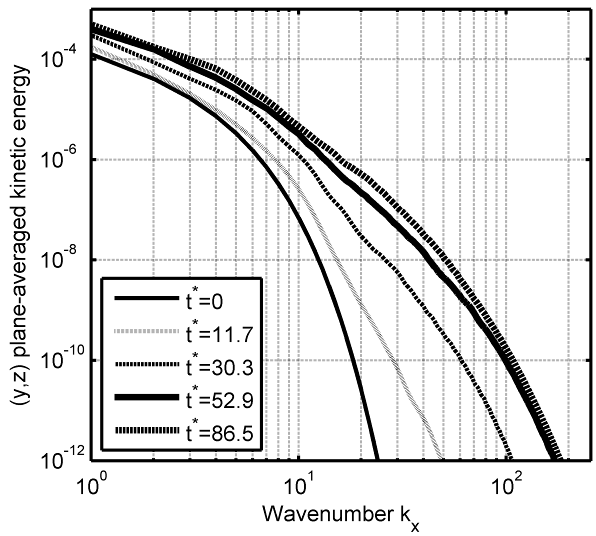

Figure 4: *Kinetic energy spectra at different times during the partial reconnection process.* $Re = 10^4$, $\Gamma_2/\Gamma_1 = 0.3$, $L = 2\pi$, $N = 512$ *and* $\nu_{hv} = 0$.

4 DIMENSIONS OF THE PERIODIC DOMAIN

To study the partial reconnection of two free vortices using a fully periodic domain, care must be taken with regards to the dimensions of the periodic box to ensure that implicit neighbours have negligible impact on the reconnection process. Hence, simulations have been carried out to quantify the impact of the neighbours in order to choose the appropriate periodic box size. Figure 7 shows the evolution of the dissipation rate for three simulations with $Re = 10^4$, $\Gamma_2/\Gamma_1 = 0.3$ and $\nu_{hv} = 0$ for cubic boxes of dimensions $L = 2\pi$, 3π and 4π. The smallest scale resolved is always the same, i.e., the ratio L/N is preserved in all three Cartesian dimensions for each simulation. In order to compare each simulation, dissipation rate is computed in the physical domain on a $(2\pi)^3$ sub-box centered in each periodic box.

One can see from Figure 7 that in this particular case, the three simulations agree very well until $t^* \approx 55$, which corresponds to the time where the traveling structures meet their periodic images for $L = 2\pi$, while they are just leaving the sub-box for $L = 3\pi$ and $L = 4\pi$. Before this time, velocity induction from neighboring vortices appears to be marginal, since changing the periodic box dimensions (thereby modifying the induction intensity) has no impact on the global flow evolution. Hence, $L = 2\pi$ can be used to study the reconnection phenomenon with negligible impact from neighbours until $t^* \approx 55$, when interactions begin to modify greatly the dynamics inside the periodic box.

Figure 7 simulations have been carried out with $Re = 10^4$. Similar analysis at higher Reynolds numbers leads to the

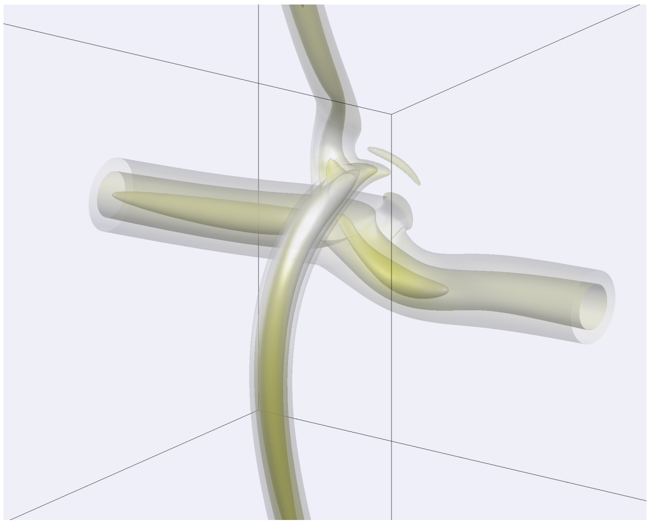

(a) $t^* = 11.7$ *: Wrapping of the secondary vortex around the main vortex.*

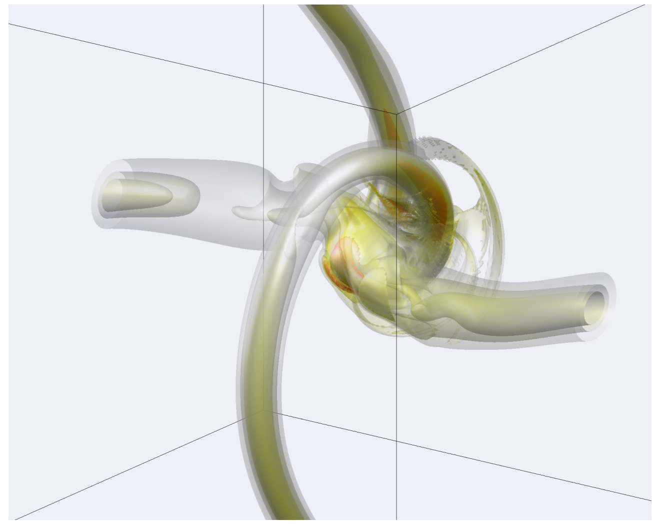

(b) $t^* = 30.3$ *: Partial reconnection between the two vortices.*

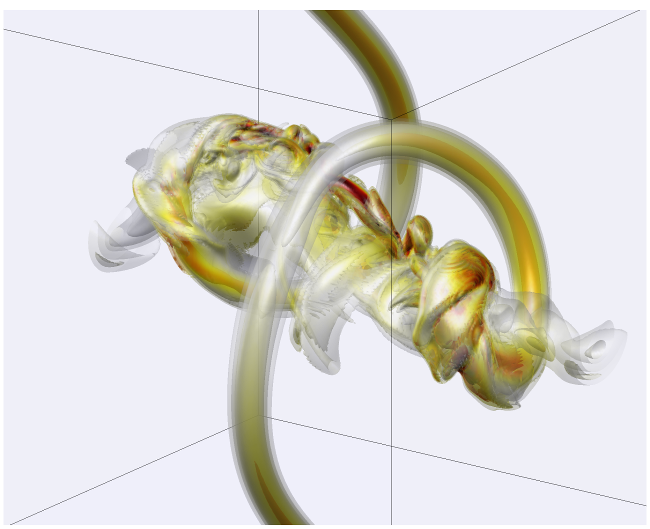

(c) $t^* = 52.9$ *: Evolution of the vortex system after the partial reconnection.*

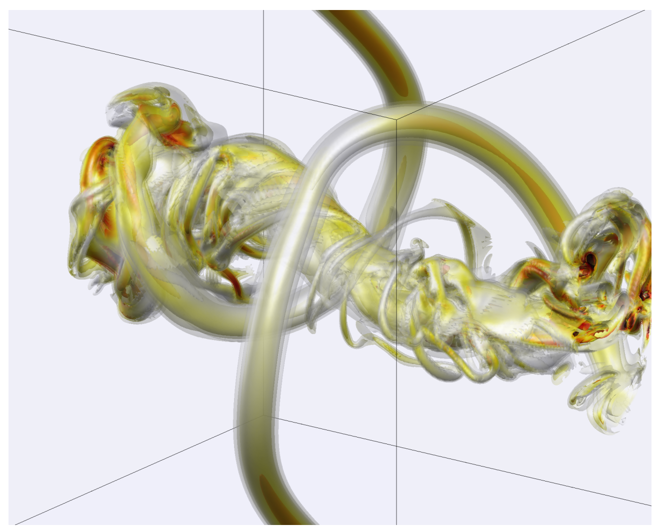

(d) $t^* = 86.5$ *: Burst of the traveling structures with their periodic images.*

Figure 5: *Local dissipation colored vorticity isosurfaces at different times.* $Re = 10^4$, $\Gamma_2/\Gamma_1 = 0.3$, $L = 2\pi$, $N = 512$ *and* $\nu_{hv} = 0$. *Vorticity isosurfaces are* $\omega^* = [0.25, 0.5, 0.75, 1.0]$. *The bolder the isosurfaces are colored, the higher is the local dissipation rate.*

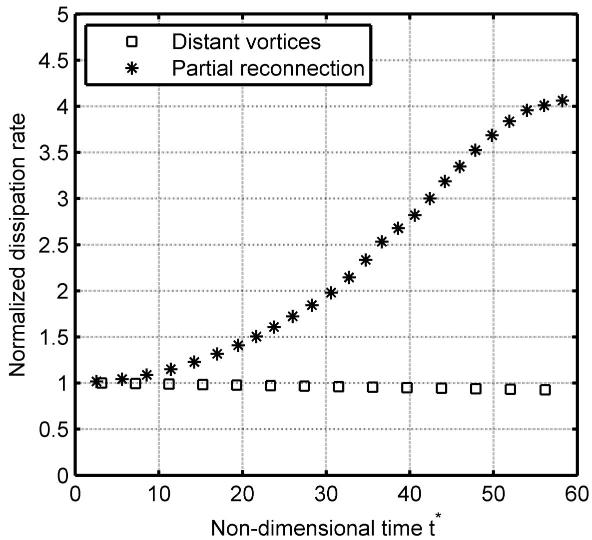

Figure 6: *Comparison of the dissipation rate for the partial reconnection between two vortices and the normal viscous dissipation of the same vortices placed far away from each other (no interaction).* $\Gamma_2/\Gamma_1 = 0.3$*,* $L = 2\pi$*,* $N = 512$*,* $\nu_{hv} = 0$ *and* $Re = 10^4$*. Dissipation rate is normalized by the initial dissipation rate in the distant vortices simulation.*

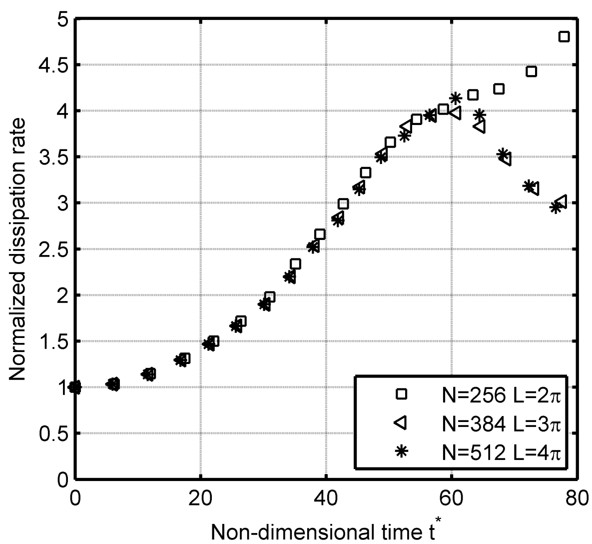

Figure 7: *Effect of the dimensions of the periodic domain on dissipation rate for three different box sizes. All boxes are cubic. Dissipation is computed on a* $(2\pi)^3$ *sub-box centered in each periodic box.* $Re = 10^4$*,* $\nu_{hv} = 0$ *and* $\Gamma_2/\Gamma_1 = 0.3$*. Dissipation rate is normalized by the dissipation rate at* $t^* = 0$.

same conclusion, i.e., $L = 2\pi$ allows thorough study of the partial reconnection process by granting a good timespan with minimal impact from neighboring vortices and a very good resolution at reasonable cost.

5 HYPERVISCOSITY TO ACHIEVE HIGHER REYNOLDS NUMBERS

The motivation to simulate partial reconnection at higher Reynolds number is well demonstrated by approximating the circulation-based Reynolds number of an aircraft obtained by assuming an elliptical load distribution

$$\Gamma = \frac{4L}{\rho\, U_\infty\, b\, \pi} \tag{9}$$

where L is the maximum take-off weight, b is the wingspan, U_∞ is the cruise speed and ρ is the density of the air.

For example, a Bombardier Q300 has approximately the following characteristics : $L = 191\ kN$, $b = 27.4\ m$ and $U_\infty = 532\ km/h$ [1], giving a circulation-based Reynolds number $Re \approx 3 \cdot 10^6$. Hence, simulation of partial reconnection at high Reynolds numbers is desirable as most civil aircrafts have a circulation-based Reynolds number ranging from 10^6 to 10^8.

Hyperviscosity is introduced as a way to overcome the limited resolution of the flow velocity spectrum resulting from finite computational resources. When increasing Reynolds number without hyperviscosity, a truncated spectrum may eventually lead to an accumulation of energy in the smallest scales, due to the inability of the discretized flow to achieve sufficient dissipation. In the context of flight safety, one could argue that only the large scales matter, being the only ones causing a possible threat. This is true, and for accurate predictions of the large structures, one must make sure that they do not get polluted by interactions with artificially boosted small scale structures. Indeed, small scales interact with larger ones through the convolution sum associated with the non-linear term in (1). In a real high-Reynolds number flow, the energy of the smaller scales is decades weaker than that of the larger ones, so small scales don't influence big structures. However, when energy is forced to accumulate at the end of the spectrum, interactions may become significant, thus possibly yielding to erroneous results. Hyperviscosity causes the flow to dissipate the smaller scales but has negligible impact on the large structures. A high-order hyperviscosity (hyperviscosity index $h = 8$ [9]) is chosen to accentuate this latter effect. Yet, in order to draw conclusions from simulations using this artifice, one has to make sure that the energy contained in the scales affected by hyperviscosity is only cascading down towards dissipation, and thus, has no impact on the evolution of the dominant structures of the flow.

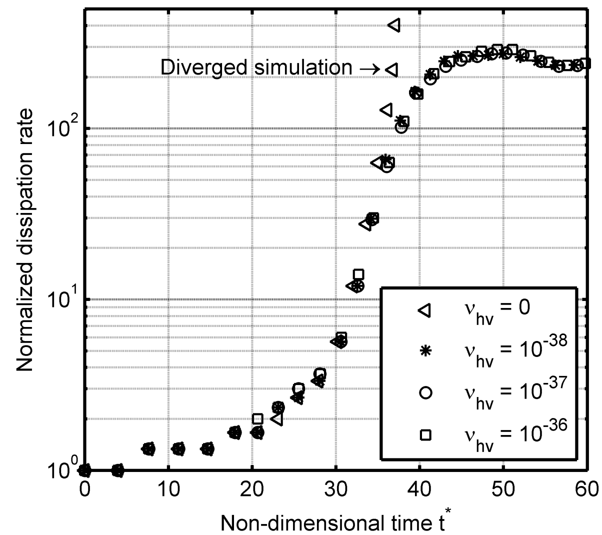

Figure 8: *Evolution of the normalized dissipation rate for different hyperviscosities.* $Re = 10^6$*,* $L = 2\pi$*,* $N = 512$ *and* $\Gamma_2/\Gamma_1 = 0.3$*. Dissipation rate is normalized by the dissipation rate at* $t^* = 0$*.*

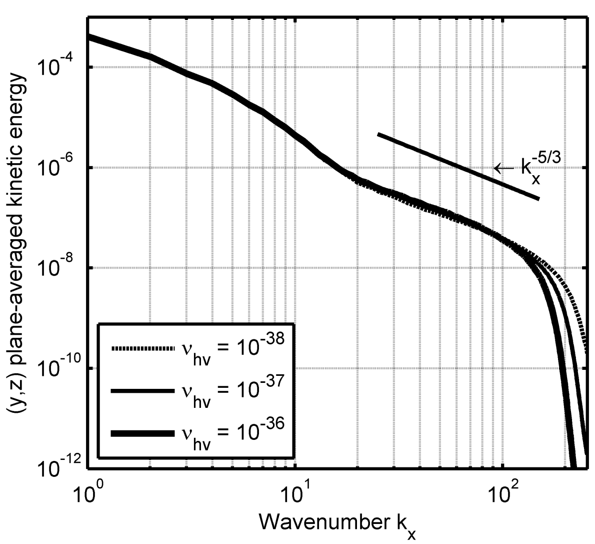

Figure 9: *Kinetic energy spectra at* $t^* = 50$ *for different hyperviscosities.* $Re = 10^6$*,* $L = 2\pi$*,* $N = 512$ *and* $\Gamma_2/\Gamma_1 = 0.3$*.*

Simulations have been carried out for $Re = 10^6$ using different hyperviscosities. For each of these simulations, evolution of the dissipation rate and the (y,z) plane-averaged kinetic energy spectrum at $t^* = 50$ is shown on Figure 8 and Figure 9 respectively. One can see from Figure 8 that the simulation without hyperviscosity diverges at $t^* \approx 35$. It is also apparent from Figure 9 that at $t^* = 50$, the tails of the kinetic energy spectra differ significantly. However, all simulations (except the one without hyperviscosity) agree well on predicting the evolution of the dissipation rate. These observations lead to the conclusion that a well-chosen hyperviscosity allows sufficient dissipation at the small scales without affecting the global evolution of the flow, thus allowing high Reynolds number simulations with limited resolution. Since $\nu_{hv} = 10^{-38}$ permits sufficient dissipation at $Re = 10^6$ and that the flow seems unaffected by higher hyperviscosities, one could argue that $\nu_{hv} = 10^{-38}$ is a good choice for $Re \leq 10^6$. This hyperviscosity is hence used for all simulations presented in the following section.

6 EFFECT OF REYNOLDS NUMBER ON PARTIAL RECONNECTION

Simulations with $L = 2\pi$, $N = 512$ and $\Gamma_2/\Gamma_1 = 0.3$ are carried out for different Reynolds numbers ranging from $Re = 10^4$ to $Re = 10^6$. Figure 10 shows the evolution of the dissipation rate for these simulations.

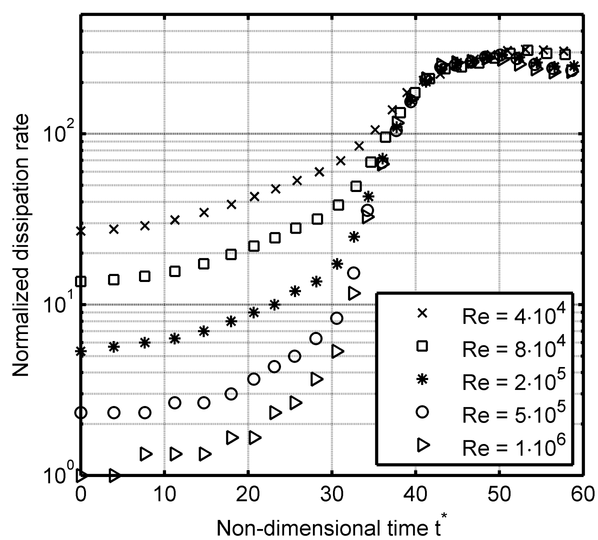

Figure 10: *Evolution of the normalized dissipation rate for different Reynolds numbers with* $L = 2\pi$*,* $N = 512$*,* $\Gamma_2/\Gamma_1 = 0.3$ *and* $\nu_{hv} = 10^{-38}$*. Dissipation rate is normalized by the initial dissipation rate at* $Re = 10^6$*.*

Dissipation rate due to the partial reconnection of two orthogonal vortices appears to be almost Reynolds-independent for $Re \gtrsim 2 \cdot 10^5$. At the beginning of the reconnection process, one can see that dissipation in the box is strongly affected by the Reynolds number. It is then a purely viscous, non-turbulent phenomenon. However, at later times, one observes that the peak dissipation rate is almost the same and occurs at the same time for the three largest Reynolds numbers. Partial reconnection being a viscous process [7], this suggests that for this initial configuration, evolution of the flow always

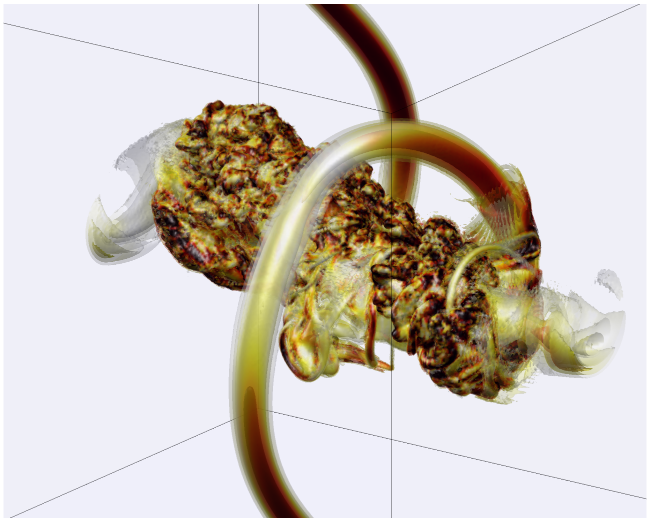

(a) $Re = 4 \cdot 10^4$

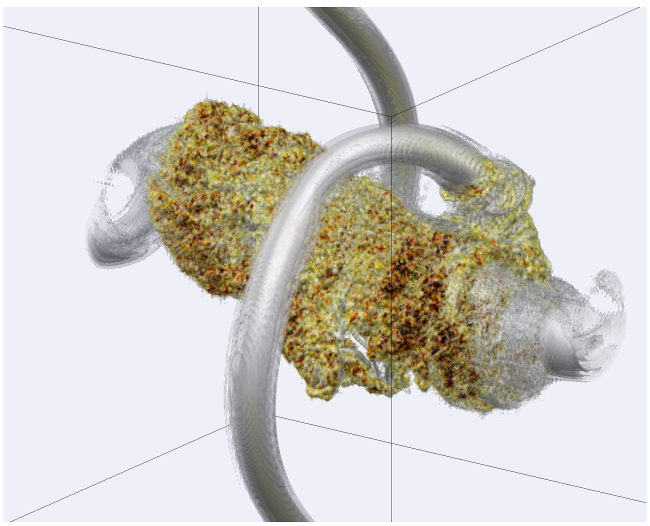

(b) $Re = 10^6$

Figure 11: *Local dissipation coloured vorticity isosurfaces at* $t^* = 50$. $\Gamma_2/\Gamma_1 = 0.3$, $L = 2\pi$, $N = 512$, $\nu_{hv} = 10^{-38}$. *Vorticity isosurfaces are* $\omega^* = [0.25, 0.5, 0.75, 1.0]$.

produces sufficiently small structures in order for the reconnection to happen, independently of the Reynolds number. These small structures are responsible for the strong increase of the dissipation rate around $t^* \approx 35$ during the partial reconnection process.

Figure 11 shows vorticity isosurfaces at $t^* = 50$ for $Re = 4 \cdot 10^4$ and $Re = 10^6$. While reaching similar dissipation rates in the heart of the reconnection process, one can see from Figure 11 that small-scale flow structures are quite different. However, the energy spectra of both simulations agree quite well in the small wavenumbers range (see Figure 12).

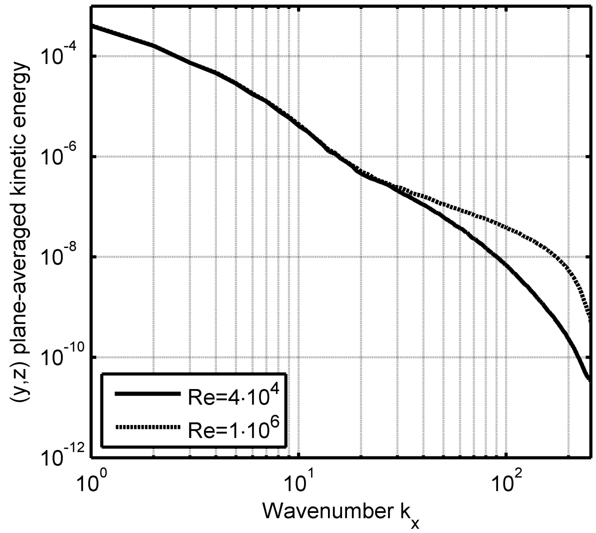

Figure 12: *Kinetic energy spectra with* $L = 2\pi$, $N = 512$, $\nu_{hv} = 10^{-38}$ *and* $\Gamma_2/\Gamma_1 = 0.3$ *at* $t^* = 50$ *for two different Reynolds numbers.*

7 CONCLUSION

To conclude, spectral methods are used to simulate the partial reconnection of two unequal-strength, orthogonal vortices. Impact of the periodical box size is assessed and it is found that a $(2\pi)^3$ box enables simulation of the reconnection process with minimal impacts from neighboring vortices until $t^* \approx 55$. Then, using this box size, the effect of hyperviscosity on the vortex dynamics at $Re = 10^6$ is examined. A hyperviscosity of $\nu_{hv} = 10^{-38}$ is chosen and is used to simulate a span of Reynolds numbers ranging from 10^4 to 10^6. Results seem to indicate that the dissipation rate due to this initial configuration of vortices becomes Reynolds-independent at $Re \gtrsim 2 \cdot 10^5$. Future work will include, in addition to a deepening of the present research, characterisation of the partial reconnection process for different circulation ratios ($0.1 \leq \Gamma_2/\Gamma_1 \leq 0.9$). Diverse ways to evaluate coherence (hence danger) of aircraft wake vortices during their decay will also be explored. In the long term, ways to accelerate the dissipation of these vortices in the context of flight safety on the outskirts of airstrips will be sought.

8 ACKNOWLEDGMENTS

Computations were performed on the Colosse supercomputer at the CLUMEQ HPC Consortium at Laval University under the auspice of Compute Canada. Authors would also like to acknowledge financial support from NSERC grant and scholarship programs.

References

[1] Bombardier Inc. Q300 fact sheet. *http://www.bombardier.com*.

[2] O. N. Boratav, R. B. Pelz, and N. J. Zabusky. Reconnection in orthogonally interacting vortex tubes: direct numerical simulations and quantifications. *Physics of Fluids*, A 4(581), 1992.

[3] C. Breitsamer. Wake vortex characteristics of transport aircraft. *Prog. Aerosp. Sci.*, 47:89–134, 2011.

[4] C. Canuto, M. Y. Hussaini, A. Quarteroni, and T. A. Zang. Spectral methods in fluid dynamics. 1988.

[5] L. Dufresne, G. Beardsell, and G. Dumas. Partial reconnection of orthogonal vortices. *Bull. Amer. Phys. Soc.*, 57, 2012.

[6] L. Dufresne and G. Winckelmans. LES of the interaction and partial reconnection of unequal strength vortices. *Intl. Conf. High Reynolds Numb. Vortex Interactions*, 2005.

[7] F. Hussain and K. Duraisamy. Mechanics of viscous vortex reconnection. *Physics of Fluids*, 23(2), 2011.

[8] W. Jackson. Wake vortex prediction: An overview. *Technical Report TP 13629E*, 30:107–138, 2001.

[9] A. G. Lamorgese, D. A. Caughey, and S. B. Pope. Direct numerical simulation of homogeneous turbulence with hyperviscosity. *Physics of fluids*, 17, 2004.

[10] J. M. Ortega, R. L. Bristol, and O. Savas. Experimental study of the instability of unequal strength counter-rotating vortex pairs. *J. Fluid Mech.*, 474:35–84, 2003.

[11] V. J. Rossow. Lift generated vortex wakes of subsonic transport aircraft. *Prog. Aerosp. Sci.*, 35:507–660, 1999.

[12] P. R. Spalart. Airplane trailing vortices. *Annual Rev. Fluid Mech.*, 30:107–138, 1998.